

# DRFormer: A Dual-Regularized Bidirectional Transformer for Person Re-identification

Ying Shu<sup>1</sup> Pujian Zhan<sup>1</sup> Huiqi Yang<sup>1</sup> Hehe Fan<sup>2</sup> Youfang Lin<sup>1</sup> Kai Lv<sup>1</sup>

## Abstract

Both fine-grained discriminative details and global semantic features can contribute to solving person re-identification challenges, such as occlusion and pose variations. Vision foundation models (*e.g.*, DINO) excel at mining local textures, and vision-language models (*e.g.*, CLIP) capture strong global semantic difference. Existing methods predominantly rely on a single paradigm, neglecting the potential benefits of their integration. In this paper, we analyze the complementary roles of these two architectures and propose a framework to synergize their strengths by a **Dual-Regularized Bidirectional Transformer (DRFormer)**. The dual-regularization mechanism ensures diverse feature extraction and achieves a better balance in the contributions of the two models. Extensive experiments on five benchmarks show that our method effectively harmonizes local and global representations, achieving competitive performance against state-of-the-art methods.

## 1. Introduction

Person re-identification (ReID) aims to retrieve a target pedestrian from the gallery given a query image. The ReID task is highly challenging due to blur, occlusions, illumination changes, and huge pose variations. We expect the model to capture holistic human body structures, **and** to attend to subtle differences between similar individuals, such as accessories and clothing textures.

Many existing ReID methods focus on discriminative fine-grained details (Zhu et al., 2022b; Hu et al., 2025) **or** global semantic features (Li et al., 2023b; Yang et al., 2024; Wei et al., 2025). On the one hand, vision foundation models (VFsMs) like DINO (Caron et al., 2021; Oquab et al.,

<sup>1</sup>Institute of Network Science and Intelligent Systems, Beijing Jiaotong University, Beijing, China <sup>2</sup>Zhejiang University, Hangzhou, Zhejiang, China. Correspondence to: Kai Lv <lvkai@bjtu.edu.cn>.

2024) have demonstrated strong capability in fine-grained feature mining. For example, a catastrophic forgetting score is employed to measure the gap between the pre-training and fine-tuning data of DINO, followed by the design of a ReID-specific module (Luo et al., 2021). On the other hand, vision-language models (VLMs) like CLIP (Radford et al., 2021) excel at extracting high-level semantic features. CLIP-ReID (Li et al., 2023b) applies CLIP to person ReID by fully exploiting its cross-modal describing ability. However, in ReID field, most existing methods rely predominantly on one of the two perspectives, neglecting the potential benefits of their integration. The potential for concurrently exploiting the local fine-grained discriminative power of DINO and the global semantic understanding of CLIP remains insufficiently explored in the current literature.

In this paper, we first investigate a question: **what specific roles DINO and CLIP play in person ReID?** 1) As shown in Figure 1 (a) and (c), we observe a clear distinction: DINO demonstrates a strong capability to attend to fine-grained local features, with attention peaks appearing along the diagonal; whereas CLIP only concentrates attention on a few fixed tokens and lacks local discriminability. 2) Figures 1 (b) and (d) illustrate the feature distributions of fine-tuned DINO and CLIP on pedestrian identities. We find that DINO features are highly overlapping and scattered, while CLIP features exhibit a clustered structure. The reason is that global semantic context can benefit inter-class separation for person ReID. The above comparisons reveal a compelling opportunity: DINO provides the necessary fine-grained texture, while CLIP ensures the essential semantic separability. Thus, the key to improving ReID performance lies in harmonizing these distinct yet complementary strengths.

Motivated by this insight, we address the pivotal question: **how to effectively combine the capabilities of DINO and CLIP?** To this end, we design our framework around two critical principles: For each individual model, we aim to enhance feature diversity, positing that more diverse information serves as a richer substrate for effective fusion. For the fusion of the two models, we prioritize effective collaboration to fully integrate their complementary advantages.

In this paper, we propose the **Dual-Regularized Bidirectional Transformer (DRFormer)**. We employ a bidirec-

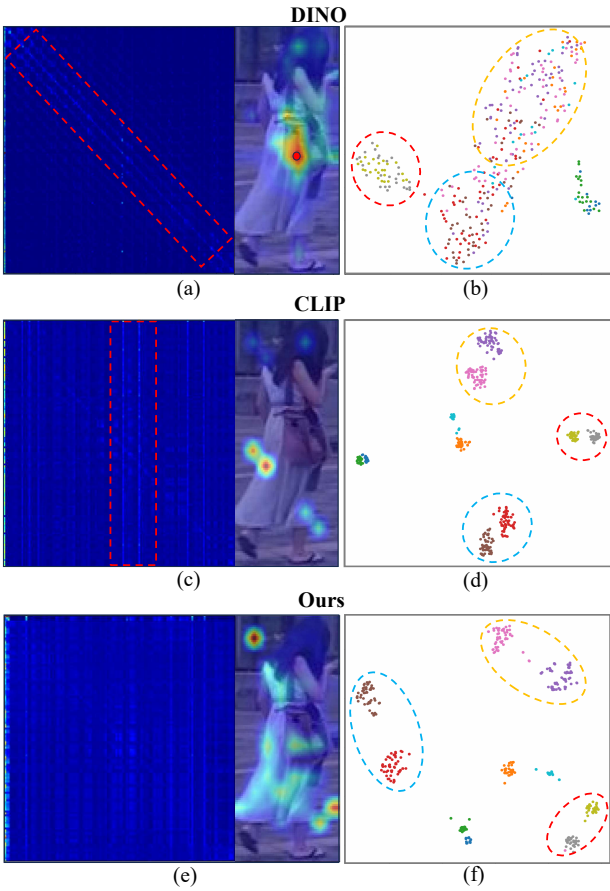


Figure 1. Comparison of attention patterns and feature distributions for DINO, CLIP and our method. The left column visualizes attention weights for all tokens and a selected token: Figure (a) shows the query image token at the red dot, while Figures (c) and (e) depict attention weights of the [CLS] token. The right column presents feature distributions of fine-tuned DINO, fine-tuned CLIP, and our method on some samples.

tional cross-attention mechanism where features from DINO and CLIP alternately serve as queries to facilitate deep interaction. Furthermore, we introduce two auxiliary regularizers. The intra-model token diversity regularizer aims to promote diverse feature learning of learnable tokens. We maximize the cosine distances of these tokens to drive the model to attend to complementary regions. The inter-model bias regularizer aims to eliminate inter-model learning suppression and achieve a better contribution ratio of the two models. Guided by our theoretical analysis, we formulate this regularizer to minimize the prediction error of each individual model. Our contributions can be summarized as:

- For the *what* question, we analyze and validate the complementary roles of DINO and CLIP: DINO captures local discriminative patterns essential for fine-grained

classification, while CLIP imposes global semantic constraints to enhance identity separability.

- For the *how* question, we propose a bidirectional transformer module and introduce two regularizers. The intra-model regularizer encourages fully exploiting diverse representations, and the inter-model regularizer balances the contributions of DINO and CLIP.
- On five person ReID datasets, our model achieves competitive performance compared with state-of-the-art ReID methods, demonstrating the effectiveness of the proposed approach.

## 2. Related Work

### 2.1. Person Re-identification

Person re-identification aims to match pedestrians across non-overlapping camera views, identifying the same identity despite pose variations and occlusions. The research landscape has evolved from CNN-based architectures to Transformer-based approaches. CNN-based methods (Sun et al., 2018; He et al., 2023) primarily focus on learning discriminative feature representations via metric learning. Nowadays, Transformer-based methods (He et al., 2021; Zhu et al., 2022a) are proposed and leverage self-attention to model long-range dependencies. The pioneering work TransReID (He et al., 2021) introduces jigsaw patches and side information embeddings to enhance feature robustness. In this paper, we propose a Transformer-based framework to achieve robust and discriminative person re-identification.

### 2.2. Large-scale Pre-training Models

Vision foundation models (VFs) (He et al., 2022; Kirillov et al., 2023; Oquab et al., 2024) and vision-language models (VLMs) (Radford et al., 2021; Jia et al., 2021; Zhai et al., 2023) are pre-trained on large-scale datasets and show strong image understanding capabilities. VFs typically act as visual backbones and are widely used in many downstream tasks (Li et al., 2023a; Wang et al., 2025). DINO (Caron et al., 2021; Oquab et al., 2024) simplifies self-supervised training by directly predicting the output of a teacher network and excels at capturing fine-grained details. MAE (He et al., 2022) significantly improves masked image modeling (MIM) for vision transformers (Dosovitskiy et al., 2021). Meanwhile, VLMs show strong generalization across diverse tasks. CLIP (Radford et al., 2021) aligns images and texts in a shared embedding space via contrastive learning, enabling effective capture of global semantic context. SigLIP (Zhai et al., 2023) further enhances this by adopting a sigmoid-based objective.

Many ReID methods are built upon existing VFs or VLMs. Based on DINO, PersonViT (Hu et al., 2025) combines

MIM with discriminative contrastive learning to extract global and local features. CLIP-ReID (Li et al., 2023b) uses prompt learning to generate text tokens for each identity and fully leverages the prior knowledge of CLIP. PromptSG (Yang et al., 2024) further improves generalization by converting image features into pseudo tokens. Different from these works that focus on only one aspect, our method aims to combine the strengths of VFM and VLMs to achieve better performance.

### 2.3. Feature Fusion Methods

Feature fusion integrates information from different levels to obtain stronger representations. The simplest approach is direct concatenation, which requires careful alignment of feature map dimensions. With the introduction of transformers, many attention-based feature fusion methods (Xu et al., 2018; Zhou et al., 2022) have been proposed. Dual attention network (DANet) is proposed to adaptively integrate local features with their global dependencies (Fu et al., 2019). GCNet (Cao et al., 2019) enhances local features using global contextual information, while significantly reducing computational complexity. For feature fusion of pre-trained models, it is more challenging due to the inherent feature-level mismatch. In other fields such as monocular depth estimation (MDE), some work (Zhang et al., 2025) guides the alignment of DINO and CLIP through text. DeCLIP (Wang et al., 2025) enhances the discriminability and spatial consistency of CLIP’s dense features by distilling attention maps of DINO, which requires training with large-scale datasets. In this paper, we achieve efficient fusion of DINO and CLIP features through a bidirectional transformer with the dual-regularization mechanism.

## 3. Proposed Method

### 3.1. Key Observations and Motivation

Before answering the question of *how* to integrate the capabilities of DINO and CLIP, we first conduct experiments to identify the key challenges in the feature fusion process. As shown in Figure 2, the challenges lie in two aspects:

#### Insufficient Feature Exploitation within DINO and CLIP.

In order to fully extract useful information from DINO and CLIP, we argue that relying solely on the classification loss is not enough. As shown in Figure 2 (a), we observe that the attention regions of different learnable tokens are almost identical. This means that different learnable tokens within the same model tend to extract relatively homogeneous features. Moreover, both tokens fail to attend to the backpack region, which can provide important cues for distinguishing similar individuals. These observations suggest that additional constraints are required to encourage diverse and complementary feature extraction within each model.

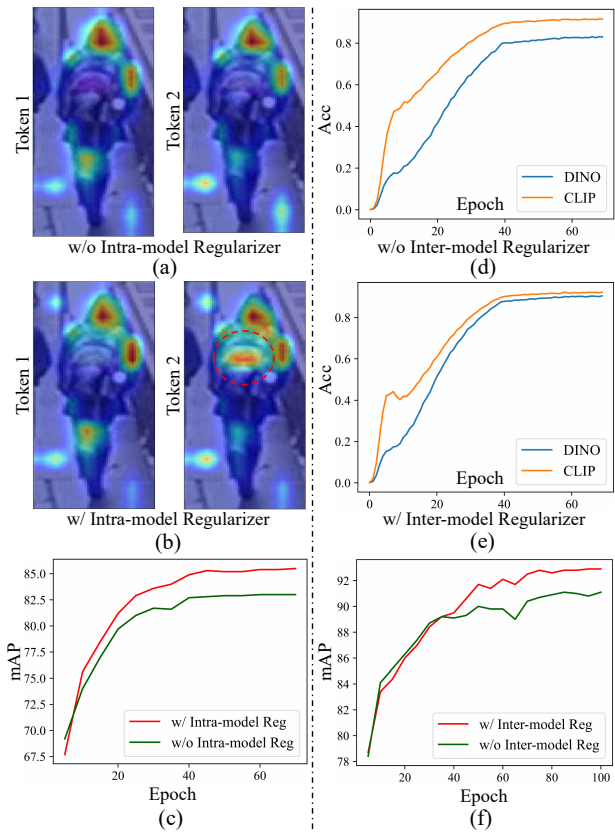


Figure 2. The left and right columns illustrate the motivation and effects of the intra-model and inter-model regularizers, respectively. Left: Figures (a) and (b) depict the attention weights of the two learnable tokens before and after the intra-model regularizer on DukeMTMC dataset. Figure (c) shows the performance gain (2.5%  $\uparrow$ ). Right: Figures (d) and (e) present the DINO and CLIP accuracy curves before and after adding the inter-model regularizer on Market-1501 dataset. Figure (f) shows the performance improvement (1.8%  $\uparrow$ ).

To encourage the tokens to extract diverse features, we introduce the **intra-model token diversity regularizer**. As shown in Figure 2 (b), the attention map of token 2 highlights the backpack region, illustrating the diversity of the learned features. Figure 2 (c) shows that the regularizer yields a performance gain of 2.5% on DukeMTMC, validating its effectiveness.

**Imbalanced Learning of DINO and CLIP.** Due to the different pre-training paradigms and datasets, the features extracted by DINO and CLIP are substantially different. Although DINO and CLIP are configured symmetrically, we hypothesize that their learning processes are inherently imbalanced. To verify this, we jointly trained both models within a unified framework, yet evaluated the performance of each branch independently on Market-1501. As shown

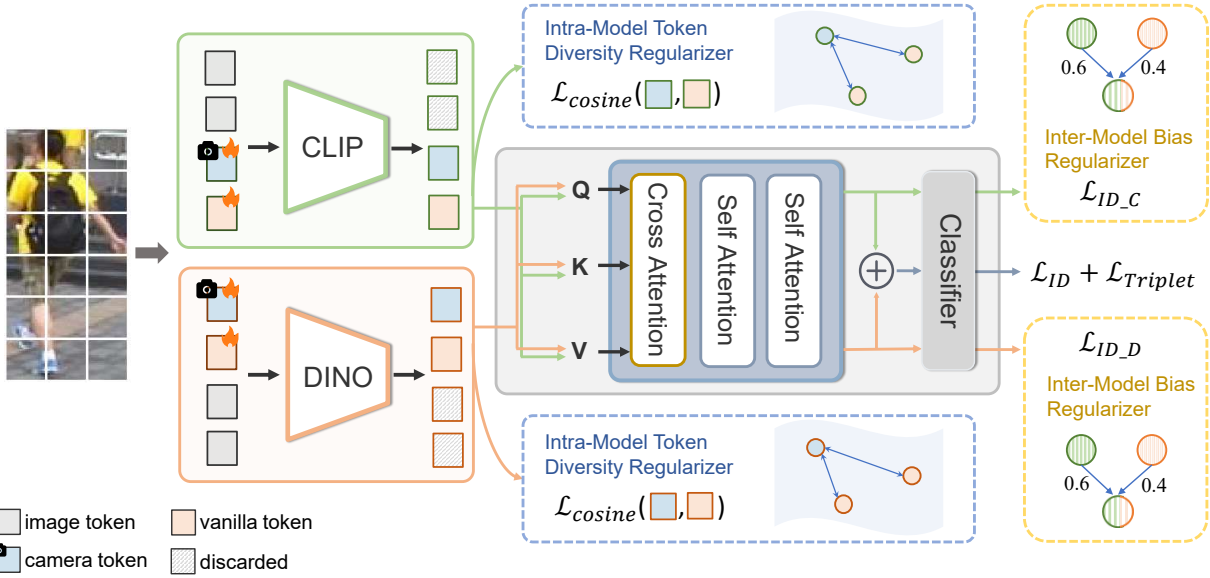


Figure 3. The framework of our method. DRFormer mainly consists of a CLIP image encoder, a DINO encoder, and a bidirectional fusion transformer. An input image is split into patches, which, along with learnable tokens, are fed separately into CLIP and DINO. The outputs of the learnable tokens from the two models serve two purposes: performing intra-model regularization and acting as queries for cross-attention. The two outputs of the fusion module are concatenated and fed into the linear classifier. Additionally, each output is also individually passed to the classifier for inter-model regularization.

in Figure 2 (d), the accuracy of CLIP increases significantly faster than that of DINO at the beginning. As the training process approaches convergence, a stable and parallel gap emerges. The experimental results reveal that the DINO and CLIP encoders exhibit different levels of learning difficulty.

To harmonize their individual contributions, we introduce the **inter-model bias regularizer**. Figure 2 (e) and (f) presents the experimental results when incorporating the inter-model regularizer. The regularizer effectively eliminates the accuracy gap between DINO and CLIP, and improves performance by a large margin on Market-1501.

### 3.2. Bidirectional Fusion Transformer

Our method aims to effectively leverage the complementary strengths of DINO and CLIP. DINO excels at fine-grained detail extraction, and CLIP captures global semantic context. We use a DINO encoder  $\mathcal{E}_{\text{DINO}}$  and a CLIP image encoder  $\mathcal{E}_{\text{CLIP}}$  to extract complementary features from the same image simultaneously. Specifically, we divide the image into  $M$  non-overlapping patches and embed them into patch-token sequences, denoted as  $\mathbf{I}_{1 \sim M}^D \in \mathbb{R}^{M \times d_D}$  for DINO and  $\mathbf{I}_{1 \sim M}^C \in \mathbb{R}^{M \times d_C}$  for CLIP, where  $d_D$  and  $d_C$  are the token embedding dimensions of the two encoders. We introduce  $N$  learnable tokens (*i.e.*,  $\mathbf{T}_{1 \sim N}^D \in \mathbb{R}^{N \times d_D}$  and  $\mathbf{T}_{1 \sim N}^C \in \mathbb{R}^{N \times d_C}$ ) for each model. These tokens are

concatenated with image tokens and then fed into two models, respectively, as shown in Equation 1 and 2.

$$[\mathbf{f}_T^D; \mathbf{f}_I^D] = \mathcal{E}_{\text{DINO}}([\mathbf{T}_1^D, \dots, \mathbf{T}_N^D; \mathbf{I}_1^D, \dots, \mathbf{I}_M^D]) \quad (1)$$

$$[\mathbf{f}_T^C; \mathbf{f}_I^C] = \mathcal{E}_{\text{CLIP}}([\mathbf{T}_1^C, \dots, \mathbf{T}_N^C; \mathbf{I}_1^C, \dots, \mathbf{I}_M^C]) \quad (2)$$

The learnable tokens are used as queries to extract useful information from two models for feature fusion. We discard the output of image tokens to reduce the computational cost. Only the output features corresponding to the learnable tokens, *i.e.*,  $\mathbf{f}_T^D$  and  $\mathbf{f}_T^C$  are fed into the fusion module.

Here, we use a bidirectional transformer to fuse the features of DINO and CLIP. The fusion module consists of one cross-attention layer and two self-attention layers. By performing bidirectional cross-attention, the semantic context of CLIP is used to query fine-grained visual details from DINO, and details captured from DINO query the global semantics encoded in CLIP. Specifically,  $\mathbf{f}_T^D$  and  $\mathbf{f}_T^C$  are alternately used as the query, while the other serves as the key and value, as shown in Equation 3 and 4. Then, we can obtain two output features, *i.e.*,  $\mathbf{H}_{D \rightarrow C}$  and  $\mathbf{H}_{C \rightarrow D}$ .  $\mathbf{H}_{D \rightarrow C}$  and  $\mathbf{H}_{C \rightarrow D}$  are two enhanced features obtained through bidirectional interaction between DINO and CLIP.

$$\mathbf{H}_{D \rightarrow C} = \text{Transformer}(\mathbf{Q} = \mathbf{f}_T^D, \mathbf{K} = \mathbf{f}_T^C, \mathbf{V} = \mathbf{f}_T^C) \quad (3)$$

$$\mathbf{H}_{C \rightarrow D} = \text{Transformer}(\mathbf{Q} = \mathbf{f}_T^C, \mathbf{K} = \mathbf{f}_T^D, \mathbf{V} = \mathbf{f}_T^D) \quad (4)$$

The outputs obtained from the two queries are concatenated and used as the input to the simple linear classifier  $f_{linear}$ . This can be formulated as follows:

$$\hat{y} = f_{linear}([\mathbf{H}_{D \rightarrow C}; \mathbf{H}_{C \rightarrow D}]) \quad (5)$$

Ultimately, we utilize the standard ReID loss, *i.e.*, the triplet loss  $\mathcal{L}_{Tri}$  and identity classification loss  $\mathcal{L}_{ID}$  (He et al., 2023), to optimize our network. The two losses are calculated as follows:

$$\mathcal{L}_{ID} = \sum_{j=1}^K -q_j \log(p_j) \quad (6)$$

$$\mathcal{L}_{Tri} = \max(d_p - d_n + \alpha, 0) \quad (7)$$

where  $q_j$  denotes the value in the target distribution,  $p_j$  represents the ID prediction logits of class  $j$ ,  $d_p$  and  $d_n$  are the feature distances of the positive and negative pairs, and  $\alpha$  is the margin of  $\mathcal{L}_{Tri}$ .

### 3.3. The Intra-model Token Diversity Regularizer

The intra-model regularizer aims to enable different learnable tokens to capture diverse representations. First, we use side information embeddings (SIE) (He et al., 2021) to incorporate camera information into the first learnable token. We add the camera-information embeddings  $\mathbf{E}_{cam}$  to the first learnable token of DINO and CLIP, respectively, as shown in Equation 8 and 9.

$$\mathbf{T}_1^D = \mathbf{T}_1^D + \mathbf{E}_{cam} \quad (8)$$

$$\mathbf{T}_1^C = \mathbf{T}_1^C + \mathbf{E}_{cam} \quad (9)$$

Then, we maximize the cosine distance, *i.e.*, minimize the cosine similarity, between the first token and vanilla learnable tokens, as shown in Equation 10 and 11. This encourages the tokens to capture diverse and complementary information. The first token can thus aggregate more comprehensive features guided by camera information, while the remaining tokens are prompted to learn viewpoint-invariant representations.

$$\mathcal{L}_{cos}^D = \frac{1}{N-1} \sum_{i=2}^N \cos(\mathbf{f}_1^D, \mathbf{f}_i^D) \quad (10)$$

$$\mathcal{L}_{cos}^C = \frac{1}{N-1} \sum_{i=2}^N \cos(\mathbf{f}_1^C, \mathbf{f}_i^C) \quad (11)$$

$$\mathcal{L}_{intra} = \mathcal{L}_{cos}^D + \mathcal{L}_{cos}^C \quad (12)$$

### 3.4. The Inter-model Bias Regularizer

The inter-model regularizer aims to find the optimal contribution ratio between DINO and CLIP. We have just concatenated the two outputs of the fusion module, *i.e.*,  $\mathbf{H}_{D \rightarrow C}$  and  $\mathbf{H}_{C \rightarrow D}$ , and input them into the classifier, as shown in Equation 5. The linear classifier can be formulated as:

$$\mathbf{z}_f = [\mathbf{H}_{D \rightarrow C}; \mathbf{H}_{C \rightarrow D}] \quad (13)$$

$$f_{linear} = \mathbf{W} \mathbf{z}_f + \mathbf{b} \quad (14)$$

Equation 14 can be further expanded to yield equations as follows:

$$f_{linear} = \mathbf{W}_D \cdot \mathbf{H}_{D \rightarrow C} + \mathbf{b}_D + \mathbf{W}_C \cdot \mathbf{H}_{C \rightarrow D} + \mathbf{b}_C \quad (15)$$

$$\mathbf{s}^D = \mathbf{W}_D \cdot \mathbf{H}_{D \rightarrow C} + \mathbf{b}_D \quad (16)$$

$$\mathbf{s}^C = \mathbf{W}_C \cdot \mathbf{H}_{C \rightarrow D} + \mathbf{b}_C \quad (17)$$

where  $\mathbf{s}^D$  denotes the logit output of the DINO and  $\mathbf{s}^C$  denotes the logit output of CLIP. As a result, the final output is the summation of  $\mathbf{s}^D$  and  $\mathbf{s}^C$ . Thus, the optimization gradient is determined by  $\mathbf{s}^D$  and  $\mathbf{s}^C$ .

Assume the contribution ratios of the two model outputs are  $w_0$  and  $w_1$ , respectively, and  $w_0 + w_1 = 1$ . The optimal solution should lead to the minimization of the generalization error  $\mathcal{L}$ , as shown in Equation 18.

$$\min_{w_0, w_1} g = \mathbb{E} \mathcal{L}(f(s), y) \quad (18)$$

$$f(s) = w_0 \mathbf{s}^D + w_1 \mathbf{s}^C \quad (19)$$

By performing a bias-variance decomposition of the generalization error (Shahhosseini et al., 2019), the solution can be rewritten as follows:

$$g = (\text{Bias}(f(s), y))^2 + \text{Var}(f(s)) + \text{Var}(\epsilon) \quad (20)$$

$$w_0 = \frac{\text{Bias}(\mathbf{s}^C, y)}{\text{Bias}(\mathbf{s}^C, y) - \text{Bias}(\mathbf{s}^D, y)} \quad (21)$$

$$w_1 = \frac{-\text{Bias}(\mathbf{s}^D, y)}{\text{Bias}(\mathbf{s}^C, y) - \text{Bias}(\mathbf{s}^D, y)} \quad (22)$$

where  $Bias(\cdot)$  is the prediction bias and  $Var(\cdot)$  is the variance of  $f(s)$ .  $Bias(s^D, y) = \mathbb{E}[s^D - y]$  and  $Bias(s^C, y) = \mathbb{E}[s^C - y]$  measures the prediction error of DINO and CLIP, respectively. However,  $w_0$  or  $w_1$  must be smaller than 0 in Equation 21 and 22, conflicting with  $w_0 > 0$  and  $w_1 > 0$ . Therefore, we cannot find the numerical solution of the equation with the constraint  $w_0 + w_1 = 1$ . More details of the theoretical derivation can be found in Appendix A.

In Equation 20, since we cannot rely solely on re-weighting to minimize the error term  $(Bias(f(s), y))^2$ , the most effective alternative is to minimize the intrinsic prediction bias of each individual model, *i.e.*,  $Bias(s^D, y)$  and  $Bias(s^C, y)$ . This motivates the following proposition:

**Proposition 3.1.** *Given a weighted fusion  $f(s) = w_0s^D + w_1s^C$  with  $w_0, w_1 > 0$  and  $w_0 + w_1 = 1$ , minimizing the generalization error requires minimizing the prediction bias of individual branches.*

Therefore, maintaining the complementary discriminative strengths of DINO and CLIP, *i.e.*, local detail modeling and global semantic understanding, respectively, is essential for achieving an effective fusion. We introduce a regularization term for each model to achieve this goal. Specifically, we copy and then feed  $\mathbf{H}_{D \rightarrow C}$  and  $\mathbf{H}_{C \rightarrow D}$  into the weight-sharing classifier  $f_{linear}$  separately, where the feature duplication is used to align input dimensions. We use the identity classification loss as the regularization loss:

$$\hat{y}_D = f_{linear}([\mathbf{H}_{D \rightarrow C}, \mathbf{H}_{D \rightarrow C}]) \quad (23)$$

$$\hat{y}_C = f_{linear}([\mathbf{H}_{C \rightarrow D}, \mathbf{H}_{C \rightarrow D}]) \quad (24)$$

$$\mathcal{L}_{inter} = \mathcal{L}_{ID\_D} + \mathcal{L}_{ID\_C} \quad (25)$$

### 3.5. Training Loss

The objective function can be formulated as follows, consisting of the ReID loss, the intra-model regularization loss, and the inter-model regularization loss:

$$L_{total} = L_{ID} + L_{Tri} + \lambda_1 L_{inter} + \lambda_2 L_{intra} \quad (26)$$

where  $\lambda_1$  and  $\lambda_2$  are hyperparameters.

## 4. Experiments

### 4.1. Experimental Setup

**Datasets and Evaluation Protocols.** In this study, we evaluate our method on five person re-identification datasets, including Market-1501 (Zheng et al., 2015), MSMT17 (Wei et al., 2018), DukeMTMC (Ristani et al., 2016), CUHK03-NP (Li et al., 2014) and Occluded-Duke (Miao et al., 2019).

Table 1. The statistics of datasets in our experiments.

Dataset	#ID	Images	Cams
Market-1501	1501	32668	6
MSMT17	4101	126441	15
DukeMTMC	1404	36411	8
CHUK03-NP	1467	13164	2
Occluded-Duke	1404	35489	8

The details of these datasets are summarized in Table 1. Following existing ReID settings, we use the mean average precision (mAP) and Rank-1 (R-1) accuracy to evaluate the performance.

**Implementation Details.** We adopt the visual encoders from DINOv2 (Oquab et al., 2024) and CLIP (Radford et al., 2021) as the backbone. We choose the ViT-B/14 for the DINO encoder and ViT-B/16 for the CLIP encoder. Both of them contain 12 transformer layers with the hidden sizes of 768 dimensions. All input images are resized to  $252 \times 126$  for DINO and  $256 \times 128$  for CLIP. The number of learnable tokens is set to 2 by default. These tokens are randomly initialized with a dimension of  $\mathbb{R}^{N \times 768}$ . The fusion transformer consists of one cross-attention layer and two self-attention layers. The final classifier is a simple linear layer that maps the features to the classification labels. We use the Adam optimizer with a learning rate of 5e-6 and consistently set  $\lambda_1 = 0.5$  and  $\lambda_2 = 5$  in equation 26 for all datasets. Since the cosine distance loss yields values in the range of  $[0, 1]$ , the coefficient  $\lambda_2$  is introduced to rescale it to the same magnitude as other loss terms. The model is trained for 70 epochs. The entire framework is implemented using PyTorch and runs on a single NVIDIA RTX4090 GPU with 24GB VRAM.

**Baseline.** The baseline builds on the pre-trained CLIP, and its visual encoder is fine-tuned via the two standard losses, *i.e.*, the triplet loss and identity classification loss.

### 4.2. Comparison with State-of-the-Art Methods

Table 2 summarizes the comparative results with ViT-based methods. DRFormer outperforms the second-best method and the baseline by a large margin on each benchmark. In particular, our method achieves 85.5% mAP and 92.5% R-1 on DukeMTMC, which are 2.6% and 2.2% higher than those of the HPL (Zhou et al., 2025) method. On Market-1501 and MSMT17 datasets, our method outperforms FlexiReID (Sun et al., 2025) by 0.8% and 11.2% in terms of mAP, respectively. Compared with PHA (Zhang et al., 2023), DRFormer outperforms it by 5.1%/5.1% mAP/Rank-1 on CUHK03-NP dataset. The experimental results demonstrate the effectiveness of our method on five datasets and highlight its strong performance.

Table 2. Comparison with state-of-the-art ViT-based methods on Market-1501, MSMT17, DukeMTMC, CUHK03-NP(labeled) and Occluded-Duke datasets. The best performance is highlighted in **bold**, and the second-best result is underlined.

Methods	References	Market-1501		MSMT17		DukeMTMC		CUHK03-NP		Occluded-Duke	
		mAP	R-1	mAP	R-1	mAP	R-1	mAP	R-1	mAP	R-1
TransReID (He et al., 2021)	ICCV'21	88.9	95.2	67.4	85.3	82.0	90.7	79.6	81.7	59.2	66.4
DINO (Caron et al., 2021)	ICCV'21	90.3	95.4	64.2	83.4	-	-	-	-	-	-
DINO+CFS (Luo et al., 2021)	Arxiv'21	91.0	96.0	66.1	84.6	-	-	-	-	-	-
DCAL (Zhu et al., 2022a)	CVPR'22	87.5	94.7	64.0	83.1	80.1	89.0	-	-	-	-
DC-Former (Li et al., 2023c)	AAAI'23	90.6	96.0	70.7	86.9	-	-	79.4	81.6	-	-
CLIP-ReID (Li et al., 2023b)	AAAI'23	89.6	95.5	73.4	88.7	82.5	90.0	81.6	80.9	<u>59.5</u>	<u>67.1</u>
AAformer (Zhu et al., 2024)	TNNLS'23	88.0	95.4	65.6	84.4	80.9	90.1	79.0	80.3	-	-
PHA (Zhang et al., 2023)	CVPR'23	90.2	<u>96.1</u>	68.9	86.1	-	-	<u>83.0</u>	<u>84.5</u>	-	-
CLIP3DReID (Liu et al., 2024)	CVPR'24	88.4	95.6	61.2	81.5	-	-	-	-	-	-
FlexiReID (Sun et al., 2025)	ICML'25	<u>92.1</u>	96.0	67.5	83.7	-	-	-	-	-	-
HPL (Zhou et al., 2025)	AAAI'26	89.8	95.9	<b>79.0</b>	<u>91.0</u>	<u>82.9</u>	<u>90.3</u>	-	-	-	-
baseline		86.4	93.3	66.1	84.4	80.0	88.8	80.0	80.5	53.5	60.8
<b>DRFormer</b>		<b>92.9</b>	<b>97.0</b>	<u>78.7</u>	<b>91.3</b>	<b>85.5</b>	<b>92.5</b>	<b>88.1</b>	<b>89.6</b>	<b>65.3</b>	<b>72.1</b>

Table 3. Ablation of the bidirectional transformer on Market-1501 dataset.

Methods	Market-1501	DukeMTMC	Market-1501	DukeMTMC
	mAP	R-1	mAP	R-1
baseline	86.4	93.3	80.0	88.8
+Concat	89.5	94.7	81.6	90.6
<b>+Transformer</b>	<b>91.1</b>	<b>96.4</b>	<b>82.8</b>	<b>91.0</b>

### 4.3. Ablation Study

**Contributions of Different Components.** As shown in Table 3, we conduct experiments on Market-1501 and DukeMTMC to study the effect of each component. ‘Concat’ refers to directly concatenating CLIP and DINO outputs, whereas ‘Transformer’ denotes feature concatenation after bidirectional transformer fusion. The experimental results show that incorporating DINO yields notable gains over the baseline, improving mAP by 3.1% on Market-1501 and 1.6% on DukeMTMC. This indicates that supplementing CLIP features with DINO’s fine-grained representations is particularly important. However, directly concatenating the features of the two results in inferior performance. Fusion transformer improves the performance by 1.6% and 1.2% in mAP on Market-1501 and DukeMTMC, respectively. The result demonstrates that the fusion module can reduce the discrepancy between DINO- and CLIP-extracted features while preserving their respective strengths.

**Ablation Study on Regularizers.** To investigate the impact of the inter- and intra-model regularizers, we conduct ablation experiments on Market-1501 and DukeMTMC, as shown in Table 4. Here, *Intra-model* denotes the intra-model regularizer, and *Inter-model* denotes the inter-model regularizer. Interestingly, on Market-1501, the inter-model regularizer contributes more to performance, improving mAP by 1.4%, whereas on DukeMTMC, the intra-model regu-

Table 4. Ablation study on the intra- and inter-model regularizers on DukeMTMC dataset.

Intra-model	Inter-model	Market-1501	DukeMTMC		
		mAP	R-1	mAP	R-1
-	-	91.1	96.4	82.8	91.0
✓	-	91.5	96.3	84.5	92.3
-	✓	92.5	96.8	83.0	91.0
✓	✓	<b>92.9</b>	<b>97.0</b>	<b>85.5</b>	<b>92.5</b>

larizer is more effective, yielding a 1.7% increase in mAP. Applying two regularizers leads to optimal results on both datasets, with improvement of 1.8%/0.6% and 2.7%/1.4% in mAP/R-1 on Market-1501 and DukeMTMC, respectively. This demonstrates the effectiveness of the two regularizers. The intra-model regularizer enhances the diversity of the features captured by the learnable tokens, and the inter-model regularizer enables a better contribution balance between DINO and CLIP.

**Ablation Study on Fine-tuned Models.** To compare the individual fine-tuning of DINO (Caron et al., 2021) and CLIP (Li et al., 2023b) with our method, we conducted experiments on Market-1501 and MSMT17. As shown in Table 5, DINO performs better on Market-1501, whereas CLIP yields superior results on MSMT17. In contrast, our method demonstrates strong performance on both datasets. Our method outperforms DINO by 2.3% on Market-1501. On the large-scale MSMT17 dataset, our method significantly outperforms the two fine-tuned models, achieving improvements of 14.5% over DINO and 12.6% over CLIP. The experimental results demonstrate the effectiveness of our method in capturing and fusing the complementary features of DINO and CLIP.

Table 5. Experiments of different fine-tuned models on Market-1501 and MSMT17 datasets.

Methods	Market-1501		MSMT17	
	mAP	R-1	mAP	R-1
DINO Fine-tuning	90.3	95.4	64.2	83.4
CLIP Fine-tuning	86.4	93.3	66.1	84.4
<b>DRFormer</b>	<b>92.9</b>	<b>97.0</b>	<b>78.7</b>	<b>91.3</b>

Table 6. The impact of various interaction modules on Market-1501. Cross and self mean cross-attention and self-attention, respectively.

Fusion Transformer	mAP	R-1
w/o Fusion Module	89.5	94.7
+1 cross-layer	91.1	96.1
+1 cross-layer & 1 self-layer	92.0	96.8
<b>+1 cross-layer &amp; 2 self-layer</b>	<b>92.9</b>	<b>97.0</b>

#### 4.4. Hyper-Parameter Analysis

**Different Structures of Bidirectional Transformer.** Table 6 summarizes the experimental results of different designs of the fusion module. As shown in Table 6, introducing a single cross-attention layer shows a notable performance improvement. With more self-attention layers, performances can be stably improved. The results demonstrate that performing the cross-attention operation leads to improved performance by facilitating the fusion of the original DINO and CLIP representations.

**Different Numbers of Learnable Tokens.** As shown in Figure 4, different datasets exhibit varying sensitivity to the number of learnable tokens. Generally, only one learnable token may limit the representation capability of the model, leading to suboptimal performance. On Market-1501 and DukeMTMC, the optimal performance is achieved with 2 and 3 learnable tokens, respectively. The above results indicate that we should consider an appropriate number of tokens. Setting too many tokens is not necessarily better.

### 5. Qualitative Analysis

**Qualitative Results of DRFormer.** Figure 1 (c) visualizes the attention maps of our method, showing its attention to the holistic body of the person. And Figure 1 (f) shows that our method enlarges the feature distances between hard samples. These results demonstrate that our approach effectively integrates the capabilities of DINO and CLIP.

**Visualization of Attention Maps.** Figure 5 visualizes the attention maps of our model on DukeMTMC and Occluded-Duke. Specifically, the first row shows images containing a single pedestrian, while the second row shows images with multiple individuals or complex backgrounds. As shown in Figure 5, our model can effectively focus on the human

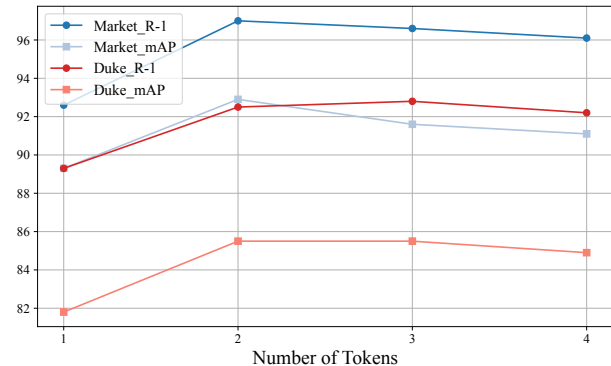


Figure 4. Visualization of the experiment results with different numbers of learnable tokens on Market-1501 and DukeMTMC datasets.

bodies and accurately localize the target pedestrians. The attention maps of our model exhibit clear boundaries with respect to the occlusions and other individuals.

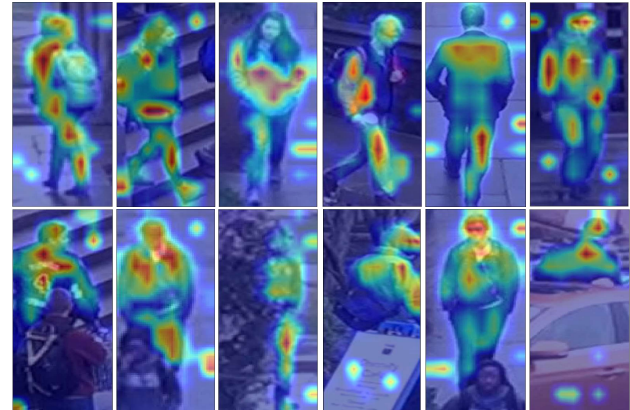


Figure 5. Visualization of attention weights on DukeMTMC and Occluded-Duke datasets.

### 6. Conclusion

In this paper, we analyze and validate the complementary roles of DINO and CLIP in person ReID. DINO effectively captures fine-grained details, while CLIP provides global semantics. To leverage their strengths, we propose a bidirectional transformer module and introduce two regularizers: an intra-model regularizer that encourages diverse feature extraction within each model, and an inter-model regularizer that balances the contributions of DINO and CLIP by theoretical guidance. Extensive quantitative and qualitative experiments confirm the effectiveness of DRFormer.

---

## Impact Statement

This paper presents work whose goal is to advance the field of Machine Learning. There are many potential societal consequences of our work, none which we feel must be specifically highlighted here.

## References

Cao, Y., Xu, J., Lin, S., Wei, F., and Hu, H. Gcnet: Non-local networks meet squeeze-excitation networks and beyond. In *2019 IEEE/CVF International Conference on Computer Vision Workshops, ICCV Workshops 2019, Seoul, Korea (South), October 27-28, 2019*, pp. 1971–1980. IEEE, 2019.

Caron, M., Touvron, H., Misra, I., Jégou, H., Mairal, J., Bojanowski, P., and Joulin, A. Emerging properties in self-supervised vision transformers. In *2021 IEEE/CVF International Conference on Computer Vision, ICCV 2021, Montreal, QC, Canada, October 10-17, 2021*, pp. 9630–9640. IEEE, 2021.

Dosovitskiy, A., Beyer, L., Kolesnikov, A., Weissenborn, D., Zhai, X., Unterthiner, T., Dehghani, M., Minderer, M., Heigold, G., Gelly, S., Uszkoreit, J., and Houlsby, N. An image is worth 16x16 words: Transformers for image recognition at scale. In *9th International Conference on Learning Representations, ICLR 2021, Virtual Event, Austria, May 3-7, 2021*. OpenReview.net, 2021.

Fu, J., Liu, J., Tian, H., Li, Y., Bao, Y., Fang, Z., and Lu, H. Dual attention network for scene segmentation. In *IEEE Conference on Computer Vision and Pattern Recognition, CVPR 2019, Long Beach, CA, USA, June 16-20, 2019*, pp. 3146–3154. Computer Vision Foundation / IEEE, 2019.

He, K., Chen, X., Xie, S., Li, Y., Dollár, P., and Girshick, R. B. Masked autoencoders are scalable vision learners. In *IEEE/CVF Conference on Computer Vision and Pattern Recognition, CVPR 2022, New Orleans, LA, USA, June 18-24, 2022*, pp. 15979–15988. IEEE, 2022.

He, L., Liao, X., Liu, W., Liu, X., Cheng, P., and Mei, T. Fastreid: A pytorch toolbox for general instance re-identification. In El-Saddik, A., Mei, T., Cucchiara, R., Bertini, M., Vallejo, D. P. T., Atrey, P. K., and Hosain, M. S. (eds.), *Proceedings of the 31st ACM International Conference on Multimedia, MM 2023, Ottawa, ON, Canada, 29 October 2023- 3 November 2023*, pp. 9664–9667. ACM, 2023.

He, S., Luo, H., Wang, P., Wang, F., Li, H., and Jiang, W. Transreid: Transformer-based object re-identification. In *2021 IEEE/CVF International Conference on Computer Vision, ICCV 2021, Montreal, QC, Canada, October 10-17, 2021*, pp. 14993–15002. IEEE, 2021.

Hu, B., Wang, X., and Liu, W. Personvit: large-scale self-supervised vision transformer for person re-identification. *Mach. Vis. Appl.*, 36(2):32, 2025.

Jia, C., Yang, Y., Xia, Y., Chen, Y., Parekh, Z., Pham, H., Le, Q. V., Sung, Y., Li, Z., and Duerig, T. Scaling up visual and vision-language representation learning with noisy text supervision. In Meila, M. and Zhang, T. (eds.), *Proceedings of the 38th International Conference on Machine Learning, ICML 2021, 18-24 July 2021, Virtual Event*, volume 139 of *Proceedings of Machine Learning Research*, pp. 4904–4916. PMLR, 2021.

Kirillov, A., Mintun, E., Ravi, N., Mao, H., Rolland, C., Gustafson, L., Xiao, T., Whitehead, S., Berg, A. C., Lo, W., Dollár, P., and Girshick, R. B. Segment anything. In *IEEE/CVF International Conference on Computer Vision, ICCV 2023, Paris, France, October 1-6, 2023*, pp. 3992–4003. IEEE, 2023.

Li, F., Zhang, H., Xu, H., Liu, S., Zhang, L., Ni, L. M., and Shum, H. Mask DINO: towards A unified transformer-based framework for object detection and segmentation. In *IEEE/CVF Conference on Computer Vision and Pattern Recognition, CVPR 2023, Vancouver, BC, Canada, June 17-24, 2023*, pp. 3041–3050. IEEE, 2023a.

Li, S., Sun, L., and Li, Q. Clip-reid: Exploiting vision-language model for image re-identification without concrete text labels. In Williams, B., Chen, Y., and Neville, J. (eds.), *Thirty-Seventh AAAI Conference on Artificial Intelligence, AAAI 2023, Thirty-Fifth Conference on Innovative Applications of Artificial Intelligence, IAAI 2023, Thirteenth Symposium on Educational Advances in Artificial Intelligence, EAAI 2023, Washington, DC, USA, February 7-14, 2023*, pp. 1405–1413. AAAI Press, 2023b.

Li, W., Zhao, R., Xiao, T., and Wang, X. Deepreid: Deep filter pairing neural network for person re-identification. In *2014 IEEE Conference on Computer Vision and Pattern Recognition, CVPR 2014, Columbus, OH, USA, June 23-28, 2014*, pp. 152–159. IEEE Computer Society, 2014.

Li, W., Zou, C., Wang, M., Xu, F., Zhao, J., Zheng, R., Cheng, Y., and Chu, W. Dc-former: Diverse and compact transformer for person re-identification. In Williams, B., Chen, Y., and Neville, J. (eds.), *Thirty-Seventh AAAI Conference on Artificial Intelligence, AAAI 2023, Thirty-Fifth Conference on Innovative Applications of Artificial Intelligence, IAAI 2023, Thirteenth Symposium on Educational Advances in Artificial Intelligence, EAAI 2023, Washington, DC, USA, February 7-14, 2023*, pp. 1415–1423. AAAI Press, 2023c.

Liu, F., Kim, M., Ren, Z., and Liu, X. Distilling CLIP with dual guidance for learning discriminative human

body shape representation. In *IEEE/CVF Conference on Computer Vision and Pattern Recognition, CVPR 2024, Seattle, WA, USA, June 16-22, 2024*, pp. 256–266. IEEE, 2024.

Luo, H., Wang, P., Xu, Y., Ding, F., Zhou, Y., Wang, F., Li, H., and Jin, R. Self-supervised pre-training for transformer-based person re-identification. *CoRR*, abs/2111.12084, 2021.

Miao, J., Wu, Y., Liu, P., Ding, Y., and Yang, Y. Pose-guided feature alignment for occluded person re-identification. In *2019 IEEE/CVF International Conference on Computer Vision, ICCV 2019, Seoul, Korea (South), October 27 - November 2, 2019*, pp. 542–551. IEEE, 2019.

Quab, M., Darcet, T., Moutakanni, T., Vo, H. V., Szafraniec, M., Khalidov, V., Fernandez, P., Haziza, D., Massa, F., El-Nouby, A., Assran, M., Ballas, N., Galuba, W., Howes, R., Huang, P., Li, S., Misra, I., Rabbat, M., Sharma, V., Synnaeve, G., Xu, H., Jégou, H., Mairal, J., Labatut, P., Joulin, A., and Bojanowski, P. Dinov2: Learning robust visual features without supervision. *Trans. Mach. Learn. Res.*, 2024, 2024.

Radford, A., Kim, J. W., Hallacy, C., Ramesh, A., Goh, G., Agarwal, S., Sastry, G., Askell, A., Mishkin, P., Clark, J., Krueger, G., and Sutskever, I. Learning transferable visual models from natural language supervision. *CoRR*, abs/2103.00020, 2021.

Ristani, E., Solera, F., Zou, R. S., Cucchiara, R., and Tomasi, C. Performance measures and a data set for multi-target, multi-camera tracking. In Hua, G. and Jégou, H. (eds.), *Computer Vision - ECCV 2016 Workshops - Amsterdam, The Netherlands, October 8-10 and 15-16, 2016, Proceedings, Part II*, volume 9914 of *Lecture Notes in Computer Science*, pp. 17–35, 2016.

Shahhosseini, M., Hu, G., and Pham, H. Optimizing ensemble weights and hyperparameters of machine learning models for regression problems. *CoRR*, abs/1908.05287, 2019.

Sun, Y., Zheng, L., Yang, Y., Tian, Q., and Wang, S. Beyond part models: Person retrieval with refined part pooling (and A strong convolutional baseline). In Ferrari, V., Hebert, M., Sminchisescu, C., and Weiss, Y. (eds.), *Computer Vision - ECCV 2018 - 15th European Conference, Munich, Germany, September 8-14, 2018, Proceedings, Part IV*, volume 11208 of *Lecture Notes in Computer Science*, pp. 501–518. Springer, 2018.

Sun, Z., Tan, L., Shen, Y., Cai, C., Sun, X., Dai, P., Cao, L., and Ji, R. Flexireid: Adaptive mixture of expert for multi-modal person re-identification. In *Forty-second International Conference on Machine Learning, ICML 2025, Vancouver, BC, Canada, July 13-19, 2025*. Open-Review.net, 2025.

Wang, J., Chen, K., Li, Y., Chen, B., Zhao, H., Qi, X., and Tian, Z. Generalized decoupled learning for enhancing open-vocabulary dense perception. *CoRR*, abs/2508.11256, 2025.

Wei, L., Zhang, S., Gao, W., and Tian, Q. Person transfer GAN to bridge domain gap for person re-identification. In *2018 IEEE Conference on Computer Vision and Pattern Recognition, CVPR 2018, Salt Lake City, UT, USA, June 18-22, 2018*, pp. 79–88. Computer Vision Foundation / IEEE Computer Society, 2018.

Wei, S., Luo, C., and Luo, Y. Improving multimodal learning via imbalanced learning. *CoRR*, abs/2507.10203, 2025.

Xu, J., Zhao, R., Zhu, F., Wang, H., and Ouyang, W. Attention-aware compositional network for person re-identification. In *2018 IEEE Conference on Computer Vision and Pattern Recognition, CVPR 2018, Salt Lake City, UT, USA, June 18-22, 2018*, pp. 2119–2128. Computer Vision Foundation / IEEE Computer Society, 2018.

Yang, Z., Wu, D., Wu, C., Lin, Z., Gu, J., and Wang, W. A pedestrian is worth one prompt: Towards language guidance person re-identification. In *IEEE/CVF Conference on Computer Vision and Pattern Recognition, CVPR 2024, Seattle, WA, USA, June 16-22, 2024*, pp. 17343–17353. IEEE, 2024.

Zhai, X., Mustafa, B., Kolesnikov, A., and Beyer, L. Sigmoid loss for language image pre-training. In *IEEE/CVF International Conference on Computer Vision, ICCV 2023, Paris, France, October 1-6, 2023*, pp. 11941–11952. IEEE, 2023.

Zhang, G., Zhang, Y., Zhang, T., Li, B., and Pu, S. PHA: patch-wise high-frequency augmentation for transformer-based person re-identification. In *IEEE/CVF Conference on Computer Vision and Pattern Recognition, CVPR 2023, Vancouver, BC, Canada, June 17-24, 2023*, pp. 14133–14142. IEEE, 2023.

Zhang, W., Liu, H., Li, B., He, J., Qi, Z., Wang, Y., Zhao, S., Yu, X., Zeng, W., and Jin, X. Hybrid-grained feature aggregation with coarse-to-fine language guidance for self-supervised monocular depth estimation. *CoRR*, abs/2510.09320, 2025.

Zheng, L., Shen, L., Tian, L., Wang, S., Wang, J., and Tian, Q. Scalable person re-identification: A benchmark. In *2015 IEEE International Conference on Computer Vision, ICCV 2015, Santiago, Chile, December 7-13, 2015*, pp. 1116–1124. IEEE Computer Society, 2015.

---

Zhou, L., Li, S., Dong, N., Tai, Y., Zhang, Y., and Li, H. Hierarchical prompt learning for image- and text-based person re-identification, 2025.

Zhou, Q., Zhong, B., Liu, X., and Ji, R. Attention-based neural architecture search for person re-identification. *IEEE Trans. Neural Networks Learn. Syst.*, 33(11):6627–6639, 2022.

Zhu, H., Ke, W., Li, D., Liu, J., Tian, L., and Shan, Y. Dual cross-attention learning for fine-grained visual categorization and object re-identification. In *IEEE/CVF Conference on Computer Vision and Pattern Recognition, CVPR 2022, New Orleans, LA, USA, June 18-24, 2022*, pp. 4682–4692. IEEE, 2022a.

Zhu, K., Guo, H., Yan, T., Zhu, Y., Wang, J., and Tang, M. PASS: part-aware self-supervised pre-training for person re-identification. In Avidan, S., Brostow, G. J., Cissé, M., Farinella, G. M., and Hassner, T. (eds.), *Computer Vision - ECCV 2022 - 17th European Conference, Tel Aviv, Israel, October 23-27, 2022, Proceedings, Part XIV*, volume 13674 of *Lecture Notes in Computer Science*, pp. 198–214. Springer, 2022b.

Zhu, K., Guo, H., Zhang, S., Wang, Y., Liu, J., Wang, J., and Tang, M. Aaformer: Auto-aligned transformer for person re-identification. *IEEE Trans. Neural Networks Learn. Syst.*, 35(12):17307–17317, 2024.

## A. Theoretical Derivation

In Section 3.4, we briefly explain the motivation for introducing the inter-model regularizer. Here, we provide a detailed derivation of the formulation.

**Dual-Model Learning.** Without loss of generality, we consider two encoders as  $\varphi_0(\theta_0, \cdot)$  and  $\varphi_1(\theta_1, \cdot)$ , where  $\theta_0$  and  $\theta_1$  are the parameters of encoders. The dataset is denoted as  $\mathcal{D} = \{x_i\}_{i=1,2,\dots,N}$ , where  $y \in 1, 2, \dots, M$ , and  $M$  is the number of categories. The representation outputs of encoders are denoted as  $\mathbf{f}_0 = \phi_0(\theta_0, x_i)$  and  $\mathbf{f}_1 = \phi_1(\theta_1, x_i)$ . The two encoders are connected through the representations by some kind of fusion method. Here, let  $\phi_f(\theta_f, \cdot)$  denotes the fusion module.  $\theta_f$  is the parameter of this module. Notably, our method employs bidirectional cross-attention for fusion. As a result, the fusion module outputs two enhanced feature representations  $\mathbf{z}_0$  and  $\mathbf{z}_1$ .

$$\mathbf{z}_0 = \phi_f(\theta_f, \mathbf{f}_0) \quad (27)$$

$$\mathbf{z}_1 = \phi_f(\theta_f, \mathbf{f}_1) \quad (28)$$

Let  $\mathbf{W} \in \mathbb{R}^{M \times (d_0+d_1)}$  and  $\mathbf{b} \in \mathbb{R}^M$  denote the parameters of the linear classifier to produce the logits output. The output of input  $x_i$  in a dual-model can be expressed as follows:

$$f(x_i) = \mathbf{W}\mathbf{z}_f + \mathbf{b} \quad (29)$$

$$\mathbf{z}_f = [\mathbf{z}_0; \mathbf{z}_1] \quad (30)$$

Let  $\mathbf{s}_i^0 = \mathbf{W}_0 \cdot \mathbf{z}_0 + \mathbf{b}_0$ , which denotes the logit output of model  $\varphi_0(\theta_0, \cdot)$ , and  $\mathbf{s}_i^1 = \mathbf{W}_1 \cdot \mathbf{z}_1 + \mathbf{b}_1$ , which denotes the logit output of model  $\varphi_1(\theta_1, \cdot)$ . As a result, the final output is the summation of  $\mathbf{s}_i^0$  and  $\mathbf{s}_i^1$ . Thus, the gradient is determined by  $\mathbf{s}_i^0$  and  $\mathbf{s}_i^1$ .

**The optimal contribution ratio for different models.** We need to find the optimal contribution ratio of different models. Generally, the optimal contribution ratio should minimize the generalization error, thus we formulate the problem as follows,

$$\min_{w_0, w_1} g = \frac{1}{N} \sum_{i=1}^{i=N} \mathcal{L}(f(x_i), y_i) \quad (31)$$

$$f(x_i) = w_0 \mathbf{s}_i^0 + w_1 \mathbf{s}_i^1 \quad (32)$$

where  $w_0 > 0$  and  $w_1 > 0$  denote the contribution of two models, respectively, and  $w_0 + w_1 = 1$ .  $\mathcal{L}(\cdot)$  measures the generalization error from prediction and ground truth. For simplification, we define  $E[f(x)] = \frac{1}{N} \sum_{i=1}^{i=N} f(x_i)$ . According to the bias-variance decomposition (Shahhosseini et al., 2019), the error between prediction and ground truth can be rewritten as follows. Here, we mainly focus on the squared term.

$$\begin{cases} g = (Bias(f(x), y))^2 + Var(f(x)) + Var(\epsilon) \\ Bias(f(x_i), y) = \mathbb{E}[f(x) - y] \end{cases} \quad (33)$$

Then, with the constraint  $w_0 + w_1 = 1$ , we get the solution of  $w_0$  and  $w_1$  as follows,

$$w_0 = \frac{Bias(s^0, y)}{Bias(s^0, y) - Bias(s^1, y)} \quad (34)$$

$$w_1 = \frac{-Bias(s^1, y)}{Bias(s^0, y) - Bias(s^1, y)} \quad (35)$$

Here, the numerical solution is meaningless since one of  $w_0$  or  $w_1$  must be smaller than 0, conflicting with  $w_0 > 0$  and  $w_1 > 0$ . Thus, when  $Bias(s^0, y)$  and  $Bias(s^1, y)$  are fixed, we can not find a reasonable combination of  $w_0$  or  $w_1$  to minimize  $Bias(\cdot)^2$ . Consequently, the only way to minimize  $Bias(\cdot)^2$  is to minimize  $Bias(s^0, y)$  and  $Bias(s^1, y)$ .

## B. Visualization of Classification Results

**Hard Pedestrian Sample Discrimination.** Figure 6 illustrates several pedestrian images with different identities, but highly similar appearances and body poses. The red dashed lines mark the differences in fine-grained details across images of different pedestrians. Our model successfully distinguished these challenging samples, demonstrating its strong capability for image understanding.

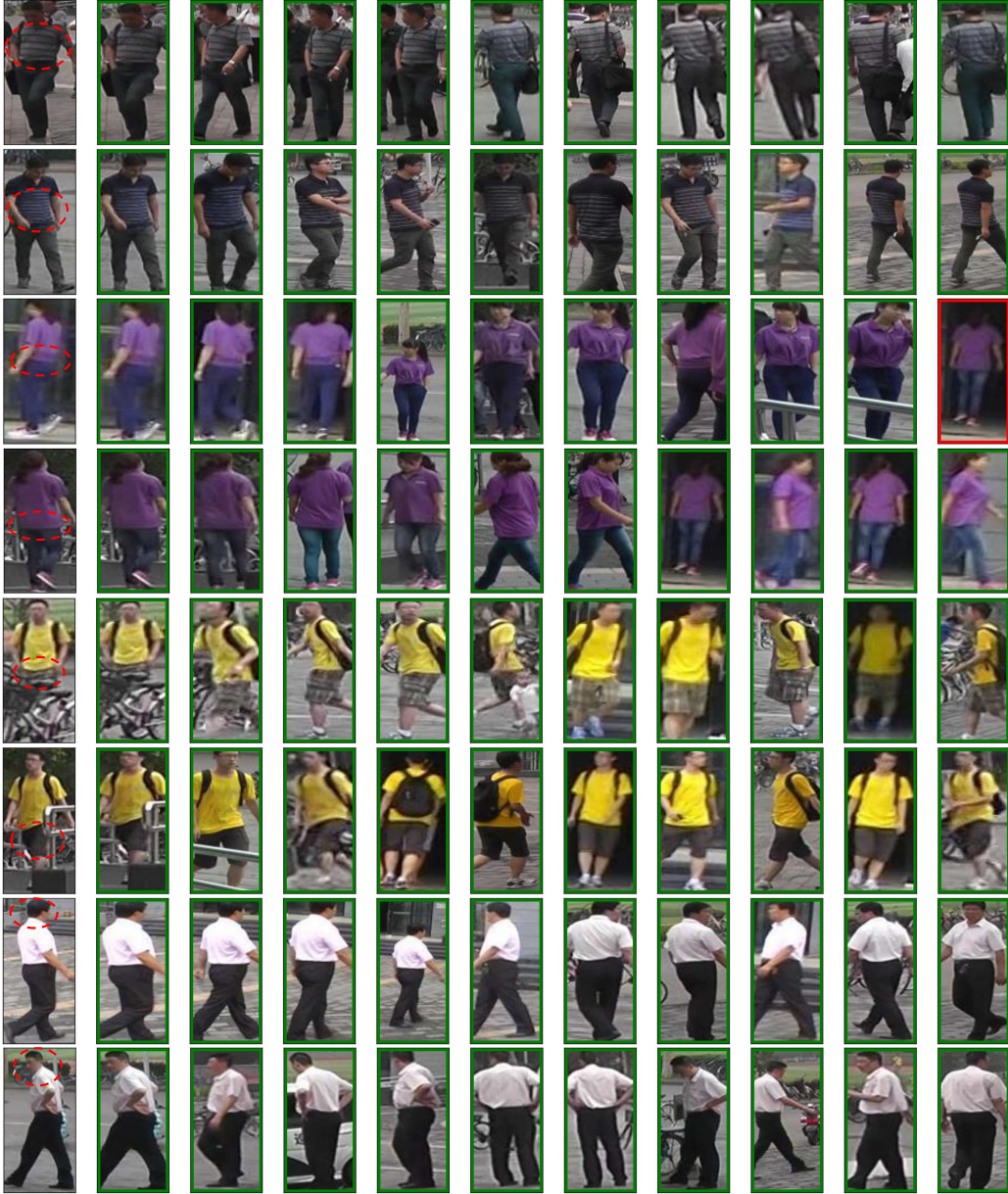


Figure 6. Classification results of highly similar samples on Market-1501.

## C. Ablation Study on Intra-model Regularizer.

**Ablation on Components of the Intra-model Regularizer.** The intra-model regularizer first applies SIE and then maximizes the cosine distance between tokens. We conduct ablation studies on these two components on the DukeMTMC and Occluded-

---

Table 7. Ablation on components of the intra-model regularizer on DukeMTMC and Occluded-Duke datasets.

Methods	DukeMTMC		Occluded-Duke	
	mAP	R-1	mAP	R-1
w/o Intra-model	83.0	91.0	64.0	72.4
+SIE	84.2	91.5	64.3	72.1
+Cosine Loss	85.5	92.5	65.3	72.3

Duke datasets. As shown in Table 7, SIE improves the mAP by 1.2% and 0.3% on DukeMTMC and Occluded-Duke, respectively. The cosine loss further boosts the performance by 1.3% and 1.0%. Overall, the cosine loss has a greater impact on performance. The experiment results validate the effectiveness of the intra-model regularizer.